ACS Combinatorial Science

Research Article

pubs.acs.org/acscombsci

# PCL/Alginate Composite Scaffolds for Hard Tissue Engineering: Fabrication, Characterization, and Cellular Activities

Yong Bok Kim and Geun Hyung Kim*

Department of Biomechatronic Engineering, College of Biotechnology and Bioengineering, Sungkyunkwan University, Suwon 110-745, South Korea

**ABSTRACT:** Alginates have been used widely in biomedical applications because of good biocompatibility, low cost, and rapid gelation in the presence of calcium ions. However, poor mechanical properties and fabrication-ability for three-dimensional shapes have been obstacles in hard-tissue engineering applications. To overcome these shortcomings of alginates, we suggest a new composite system, consisting of a synthetic polymer, poly(ε-caprolactone), and various weight fractions (10−40 wt %) of alginate. The fabricated composite scaffolds displayed a multilayered 3D structure, consisting of microsized composite struts, and they provided a 100% offset for each layer. To show the feasibility of the scaffold for hard tissue regeneration, the composite scaffolds fabricated were assessed not only for physical properties, including surface roughness, tensile strength, and water absorption and wetting, but also in vitro osteoblastic cellular responses (cell-seeding efficiency, cell viability, fluorescence analyses, alkaline phosphatase (ALP) activity, and mineralization) by culturing with preosteoblasts (MC3T3-E1). Due to the alginate components in the composites, the scaffolds showed significantly enhanced wetting behavior, water-absorption (∼12-fold), and meaningful biological activities (∼2.1-fold for cell-seeding efficiency, ∼2.5-fold for cell-viability at 7 days, ∼3.4-fold for calcium deposition), compared with a pure PCL scaffold.

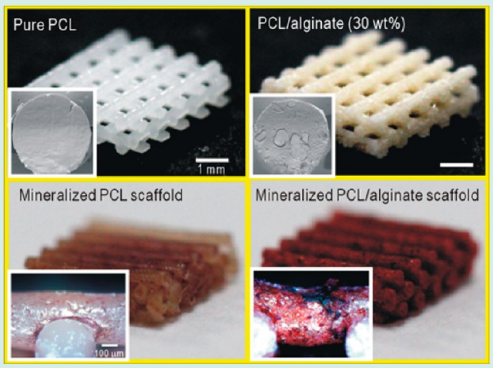


**KEYWORDS:** *bone, tissue engineering, composite scaffolds, alginates, poly(ε-caprolactone)*

## INTRODUCTION

Biomedical synthetic and natural polymers and their composite scaffolds have been used widely in hard tissue regeneration.[1−3] Generally, scaffolds should resemble an extracellular matrix (ECM) and thus require highly porous structures and three-dimensional (3D) shapes that readily allow cell attachment, proliferation, differentiation, and vascularization.[4,5] Additionally, they need nontoxic byproducts in degradation and appropriate temporary mechanical stability.[4,6]

Recently, synthetic biomedical scaffolds have evolved from a simple cell attachment and proliferation supporter to multifunctional platforms, such as scaffolds having an artificial vascular-like structure,[7] releasing various growth factors,[8,9] and containing embedded bioactive materials (e.g., collagen, chitosan, SIS, silk fibroin, alginate).[10] To generate these types of scaffold, several methods (e.g., solvent casting, particle leaching, freeze-drying, and electrospinning) have been used.[2] However, the scaffolds fabricated using these methods have several limitations, such as residual solvents, which may have toxic and carcinogenic effects,[11,12] inhomogeneous mechanical strength, and low controllability of the microinternal pore structure (insufficient interconnectivity between pores and inability to spatially design the internal channels),[12] which affect cell shape modeling and the expression of genes related to cell growth.[10,13]

To overcome these problems, a direct dispensing system has been investigated for fabrication of 3D biocomposite scaffolds with defined internal pore structures.[14−16] Its flexibility in controlling the mechanical properties of the biocomposite and the ease of forming the desired 3D shapes suggest its promise compared to previous "conventional" scaffold fabrication methods.[17,18] Generally, unlike synthetic polymers, natural biopolymers have low toxicity during degradation, structural similarities to macromolecular-based human tissue components, and good biocompatibility.[19,20]

In particular, alginates are a promising material for the fabrication of porous 3D composite scaffolds because of good biocompatibility, controllable degradation, and rapid gelation using calcium chloride.[21−23] The main disadvantages of alginates for hard tissue engineering are their low mechanical strength and poor controllability of the microinternal architecture because of the poor mechanical properties and excessive hydrophilicity.[24]

To address these limitations, several researchers have combined alginates with other biomaterials (bioceramics and synthetic polymers) to produce biocomposites that provide both the biological advantages of alginates and greater mechanical strength because of the reinforcing material.[24−26] Luo et al. suggested a biphasic organic−inorganic scaffold, which consisted of alginate and calcium phosphate cement.[27]

**Received:** February 26, 2014
**Revised:** November 30, 2014
**Published:** December 26, 2014





DOI: 10.1021/co500033h
ACS Comb. Sci. 2015, 17, 87−99

The fabricated composite scaffold showed significantly increased mechanical properties, compared with pure alginate, and its cytocompatibility was demonstrated by culturing human mesenchymal stem cells (hMSCs) for 3 weeks.[27]

Additionally, in our previous work, we produced a core (PCL)-shell (alginate/collagen) scaffold[28] and a hybrid scaffold interdigitated with PCL struts and preosteoblasts-laden alginate struts,[29] showing the use of alginates as a bioactive material in a biocomposite system. The core−shell composite scaffold displayed outstanding mechanical properties, compared with a pure collagen/alginate scaffold, and also significantly improved biological activities (cell-seeding efficiency, cell-proliferation, ALP activity and calcium deposition) compared with those of a pure PCL scaffold. However, achieving a homogeneous structure of the core (PCL)−shell (alginate/collagen) in the whole scaffold was difficult because of the complex fabrication process. Also, the structural integrity of the scaffold during the long cell culture process was too low because of the fast degradation of the shell component (collagen/alginate).

We have also fabricated electrospun PCL/alginate composite scaffolds which demonstrated improved hydrophilic behavior and high cellular responses (cell viability and calcium mineralization) relative to a pure electrospun PCL scaffold.[30] However, the electrospun composite has significant disadvantages, particularly a severe limitation on the amount of alginate in the composite (∼5 wt %) that allows electrospinning to be performed, and the presence of residual solvents in the resulting composites.

In this study, we suggest another easy and effective strategy to produce a PCL/alginate biocomposite, which has appropriate mechanical properties, high structural integrity for long cell culture periods, and good biological responses, without using any toxic chemicals. Here we used PCL as a matrix material and incorporated up to 40 wt % alginate in a melt-plotting system. PCL is commonly employed in tissue regeneration because of its good mechanical properties, appropriate miscibility with a large range of other biopolymers and bioceramics, and its biodegradability and biocompatibility.[31,32] The process described here provided multilayered and mesh-structured PCL/alginate biocomposites, which were evaluated for physical properties (including surface morphology, tensile modulus, and water absorption and wetting) and biological responses by culturing preosteoblasts (MC3T3-E1). The optimized composites showed slightly lower elastic moduli compared with a pure PCL scaffold and considerable biocompatibility, evidenced by cell-seeding efficiency, cell-proliferation, ALP activity, and calcium deposition.

## EXPERIMENTAL PROCEDURES

**Materials and Procedure for Fabrication of Multilayered PCL/Alginate Scaffolds.** Poly($\varepsilon$-caprolactone; PCL, Cat. No. 440 744, density = 1.135 g/cm$^3$, melting temperature = 60 °C) was obtained from Sigma-Aldrich (USA). PCL has an average molecular weight ($M_n$) of 60 000 g/mol. Low-viscosity and high G-content nonmedical grade LF10/60 alginate (FMC BioPolymer, Drammen, Norway) was used as a dispersed material. To cross-link the alginate solution, $CaCl_2$ (Sigma-Aldrich) was used.

To obtain a homogeneous alginate distribution in the composites, the mixture of PCL powders and alginate powders was injected into a heating cylinder at 130 °C, and the melted PCL/alginate was extruded through a heated 250-$\mu$m nozzle. The extruded struts were reground in a freezer mill to obtain a uniform distribution of alginate in the composites. The reground PCL/alginate mixtures were transferred to the heating barrel of the plotting system, which was connected to a three-axis robot system. For the first layer, the perpendicular struts were plotted and for the second layer, the struts were plotted with a 100% offset value compared to the previous layer. The third layer was plotted with the same geometry as the first layer. The speed of the plotter nozzle was set at 5 mm/s, but the applied pneumatic pressure and process temperature differed for the mixture ratio of PCL and alginate because each mixture had unique rheological properties. To cross-link the alginate, the composite scaffolds were immersed in 5 wt % of $CaCl_2$ solution for 20 min, followed by washing in demineralized water (three times for 30 min).

In this work, we designated the pure PCL and various composites with various alginate weight fractions (10, 20, 30, 40 wt %) as "PP," "PA-10," "PA-20," "PA-30," and "PA-40," respectively.

**Physical Characterization of the Composite Scaffolds.** PCL/alginate composites were used to assess the rheological properties (complex viscosity) with a rotational rheometer (Bohlin Gemini-HR-nano, Malvern Instruments, Surrey, UK) equipped with a cone-and-plate geometry (diameter, 20 mm; cone angle, 4° and gap size, 150 $\mu$m). Dynamic frequency sweeps were conducted by applying 2% strain within the linear viscoelastic region over a frequency range between 0.1 and 10 Hz for dynamic shear measurements. All dynamic experiments were conducted at 120 °C.

Thermogravimetric analysis (TGA) was performed under nitrogen using a TGA-2050 (TA-Instruments, New Castle, DE, USA). A typical sample mass of 10 mg was heated from 25 to 750 °C at a ramp rate of 20 °C/min. Differential scanning calorimetry (DSC) thermograms were obtained using a DSC-2010 instrument (TA-Instrument, USA). The specimens (3 mg) were placed in an aluminum pan with a heating range of 20−180 °C at a rate of 10 °C/min. The melting temperature ($T_m$) and melting enthalpy ($\Delta H$) of the pure PCL and composites were determined from the first heating scan.

A scanning electron microscope (SEM, SNE-3000M, SEC Inc., South Korea) was used to characterize the surface morphology of the composite scaffolds. Additionally, the morphologies of cells were evaluated at various time periods after culture by SEM. To measure surface roughness qualitatively, a surface roughness tester (Nanoview m4151p, South Korea) was used. The 3D profiles of the various surface roughness values ($R_a$, $R_t$, RMS) were obtained using the roughness tester with phase-shifting interferometry, a common optical technique for noncontact surface profilometry.

Water absorption was calculated by weighing the samples before and after soaking in distilled water for 12 h. The percentage increase in water absorption was calculated as (%) = $(W_{12h} - W_o)/W_o \times 100$, where $W_{12h}$ was the weight of samples after 12 h, and $W_o$ was the original weight of the sample at baseline. To evaluate biodegradability, the initial weight ($W_o$) of the samples was measured and they were then immersed in PBS solution and maintained at 37 °C in an incubator. After various time periods, the weight ($W_f$) was measured. The percentage weight loss was calculated as weight loss (%) = $[(W_o - W_f)/W_o] \times 100$.

To assess mechanical properties, we used two different sample geometries (single struts and scaffolds). For measuring the mechanical properties of the single struts of pure PCL and various composites, we used struts of a similar diameter (351 ±


DOI: 10.1021/co500033h
ACS Comb. Sci. 2015, 17, 87−99

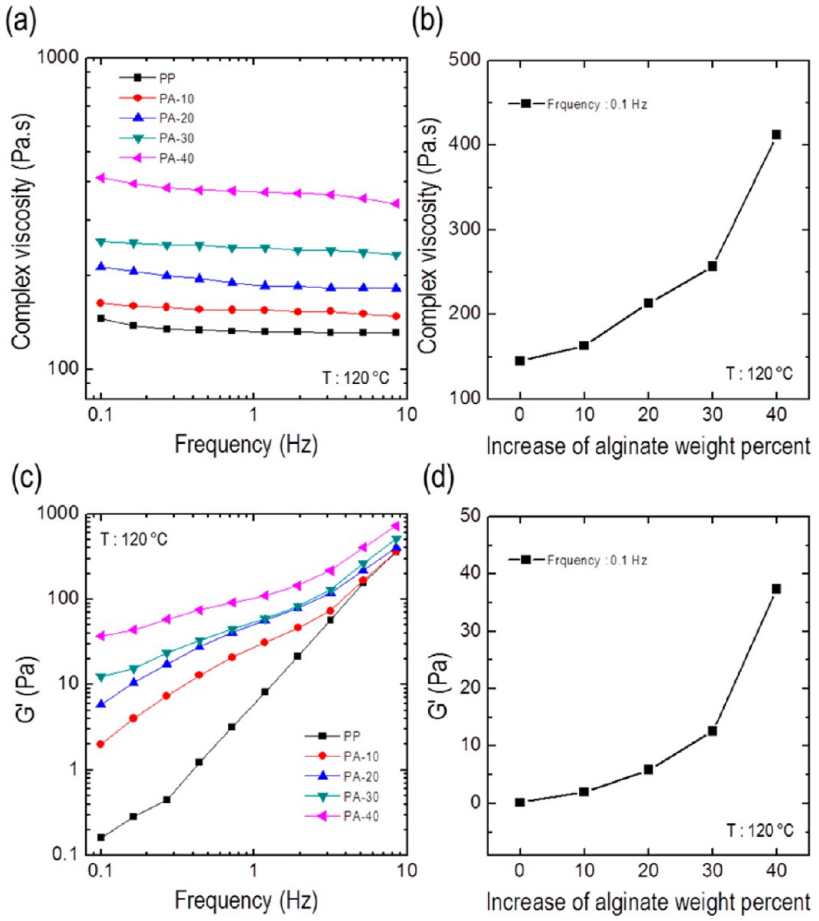


**Figure 1.** Rheological results for pure PCL (PP) and PA composites (PA-10, PA-20, PA-30) with 10, 20, and 30 wt % alginate at 120 °C. (a) Complex viscosity according to alginate concentration and (b) comparison of complex viscosity at 0.1 Hz. (c) Storage moduli ($G'$) of pure PCL and various PA composites and (d) comparison of $G'$ at 0.1 Hz.

21 $\mu$m). Also, some scaffolds were cut into small strips (8 × 20 mm$^2$). A tensile test was carried out using a tensile instrument (Top-tech 2000; Chemilab, Kyunggi-Do, South Korea). The tensile test was performed in a "wet" state. For the test, a single strut and scaffold were prewetted with phosphate-buffered saline (PBS) for 12 h at 37 ± 5 °C and then measured in the wet state. The stress−strain curves were recorded at a stretching speed of 2 mm/s. All values are expressed as means ± standard deviation ($n$ = 5).

**Biological Characterization of the Composite Scaffolds.** To assess compatibility with in vitro cell culture, samples (5 × 5 mm$^2$) were sterilized with 70% ethanol and ultraviolet (UV) light, and then placed in culture medium overnight. Mouse preosteoblast cells (MC3T3-E1) of passage five in pure PCL and composite scaffolds were cultured in 24-well plates in $\alpha$-minimum essential medium (Life Sciences, USA) containing 10% fetal bovine serum (Gemini Bio-Products, USA) and 1% antibiotic (Antimycotic, Cellgro, USA). The cells were seeded onto scaffolds at a density of 1 × 10$^5$ per sample, and incubated at 37 °C in an atmosphere of 5% $CO_2$. The medium was changed every second day.

To measure cell-seeding efficiency, we followed the method of Sobral et al.[33] Briefly, the seeded cells were left in the scaffolds during 12 h to provide sufficient time for the cells to attach to the scaffolds. After 12 h, the scaffolds were removed and the cells remaining in the wells were counted. The efficiency for each scaffold was calculated by taking into account the initial number of cells that were seeded and the residual number of cells in the respective well after 12 h. Five specimens of each composite scaffold were used. The seeding efficiency was calculated as[33] seeding efficiency (%) = (cells added to scaffold−cells in wells)/(cells added to scaffold) × 100.

Cell viability was determined using the MTT assay (Cell Proliferation Kit I, Boehringer Mannheim, Mannheim, Germany). This assay is based on cleavage of the yellow tetrazolium salt MTT by mitochondrial dehydrogenases in viable cells to produce purple formazan crystals. Cells on the scaffold were incubated with 0.5 mg mL$^{-1}$ MTT for 4 h at 37 °C, and the absorbance at 570 nm was measured using a microplate reader (EL800; Bio-Tek Instruments, Winooski, VT). Five samples were tested for each incubation period, and each test was performed in triplicate.

ALP activity was assayed by measuring the release of $p$-nitrophenol (pNP) from $p$-nitrophenyl phosphate (pNPP). The scaffolds seeded with MC3T3-E1 were rinsed gently with phosphate-buffered saline (PBS) and incubated for 10 min in Tris buffer (10 mM, pH 7.5) containing 0.1% Triton X-100 surfactant. Then, the lysate (100 $\mu$L) was added to the wells of 96-well plates containing 100 $\mu$L of pNPP solution, prepared using an ALP kit (procedure no. ALP-10; Sigma-Aldrich). In the presence of ALP, pNPP is converted to pNP and inorganic phosphate. ALP activity was determined from the absorbance at 405 nm using a microplate reader (Spectra III; SLT Lab Instruments, Salzburg, Austria). The optical density (OD) of


DOI: 10.1021/co500033h
ACS Comb. Sci. 2015, 17, 87−99

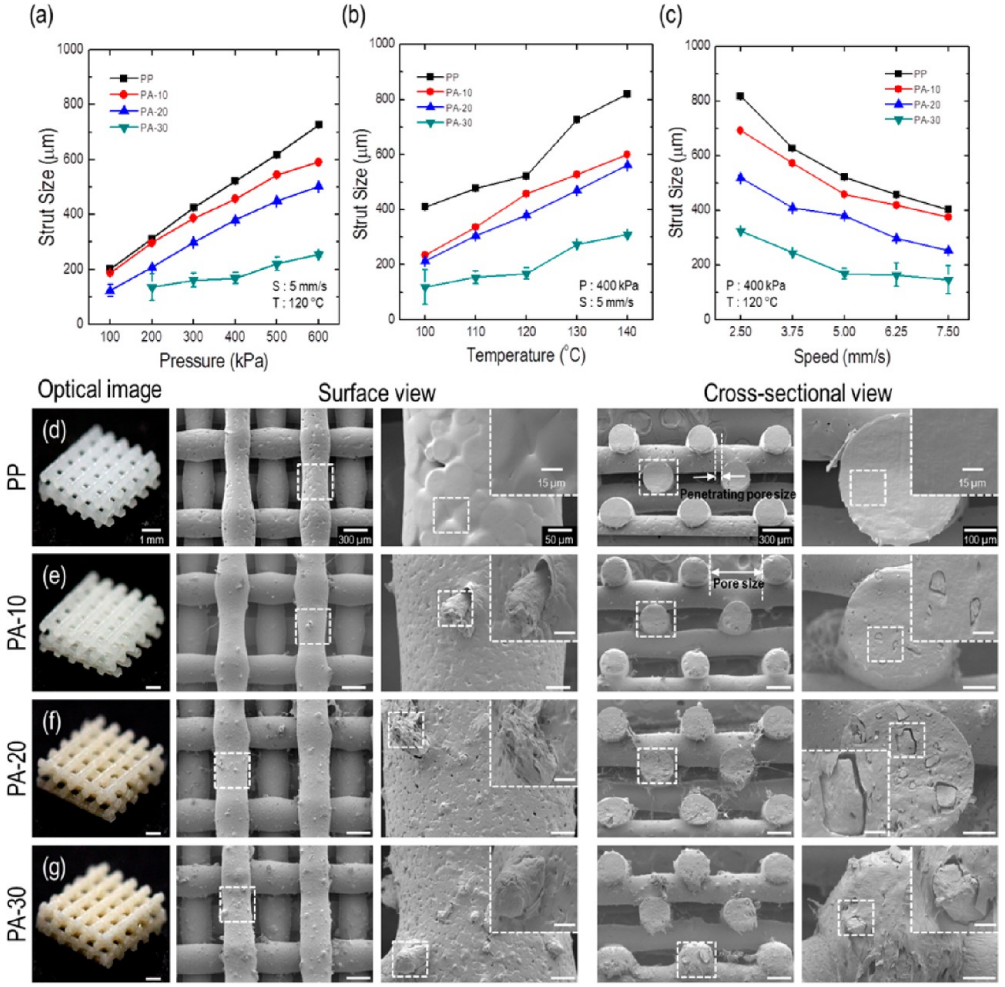


**Figure 2.** Effects of processing ((a) pressure, (b) temperature, and (c) speed) on the fabricated struts of pure PCL and PA-composites. Three-dimensional optical shapes and surface and cross-sectional SEM images of (d) pure PCL and (e–g) PA-composites.

ALP activity was normalized relative to the total protein content (OD value).

Calcium mineralization was determined by alizarin red S staining of MC3T3-E1 cells in 24-well plates. The cells were cultured in $\alpha$-MEM containing 50 $\mu$g mL$^{-1}$ vitamin C and 10 mM $\beta$-glycerophosphate. The cells were then washed three times with PBS, fixed in 70% (v/v) cold ethanol (4 °C) for 1 h, and air-dried. The ethanol-fixed specimens were stained with 40 mM alizarin red S (pH 4.2) for 1 h and washed three times with purified water. The specimens were then destained with 10% cetylpyridium chloride in 10 mM sodium–phosphate buffer (pH 7.0) for 15 min. An optical microscope was used to observe the staining. The optical density (OD) of mineralization was normalized relative to the total protein content (OD value).

The total protein content was measured using the bicinchoninic acid (BCA) protein assay (Pierce Kit; Thermo Scientific). Cell/scaffold samples were assayed after culturing for 7 and 14 days. Specimens were washed with PBS and lysed with 1 mL of 0.1% Triton X-100. An aliquot of the lysate (25 $\mu$L) was added to 200 $\mu$L of BCA working reagent, and the mixture was incubated for 30 min at 37 °C. The absorbance at 562 nm was determined using a plate reader.

**Fluorescence Images.** After 1 and 7 days in cell culture, the scaffolds were exposed to 0.15 mM calcein AM and 2 mM ethidium homodimer-1 for 45 min in an incubator to permit observation of live and dead cells. The stained specimens were visualized under a microscope (TE2000-S; Nikon, Tokyo, Japan) equipped with an epifluorescence attachment and a SPOT RT digital camera (SPOT Imaging Solutions, Sterling Heights, MI). Stained images were captured; green and red indicated live and dead cells, respectively. The ImageJ software (National Institutes of Health, Bethesda, MD) was used to count live cells.

After 14 and 21 days of cell culture, the scaffolds were subjected to diamidino-2-phenylindole (DAPI) fluorescence staining to detect cell nuclei. Phalloidin (Invitrogen, Carlsbad, CA) staining was also performed to visualize the actin cytoskeleton of proliferated cells. A laser-scanning microscope (LSM510; Carl Zeiss, Oberkochen, Germany) was used to obtain the images.

**Statistical Analyses.** All data are presented as means ± standard deviation. Statistical analyses were performed using the SPSS software (version 20.0; SPSS, Inc., Chicago, IL), and included single-factor analyses of variance (ANOVA). In all analyses, $P$ values < 0.05 were considered to indicate statistical significance. "NS" indicates no statistically significant difference.

## RESULTS AND DISCUSSION

**Rheological Properties of PCL/Alginate Biocomposites.** The rheological properties of the melted pure PCL and PCL/alginate composites were measured. As shown in Figure



DOI: 10.1021/co500033h
ACS Comb. Sci. 2015, 17, 87–99

**Table 1. Processing Conditions for the PCL and PCL/Alginate Composite Scaffolds**

| | PP | PA-10 | PA-20 | PA-30 |
|---|---|---|---|---|
| total processing time (min) (overall size 20 × 20 × 1.5 $mm^3$) | 8 | 8 | 8 | 8 |
| nozzle moving velocity (mm $s^{-1}$) | 5 | 5 | 5 | 5 |
| processing temperature (°C) | 120 | 120 | 120 | 140 |
| pneumatic pressure (kPa) | 230 | 260 | 360 | 540 |
| outer nozzle diameter ($\mu$m) | 350 | 350 | 350 | 350 |

1a, the complex viscosity of pure PCL and the composites exhibited roughly Newtonian behavior in the measured frequency range, and the viscosity was enhanced exponentially with the increase in alginate weight fraction (Figure 1b). The storage modulus ($G'$) of the composites was significantly higher than that of pure PCL, and also the increase in the modulus was highly dependent on the alginate composition (Figure 1c, d). From the rheological properties of PCL and the composites, we can estimate that to obtain homogeneous PCL/alginate struts extruded from the nozzle, the processing conditions (pneumatic pressure applied in the extruding nozzle and processing temperature) should have different values. Additionally, as shown in Figure 1b, d, the complex viscosity and storage modulus of the 40 wt % alginate in the composite were too high versus the other weight fractions of alginate. If we assume that the viscosity of the composites follow a Newtonian flow, the increase in the shear viscosity in the Hagen−Poiseuille equation can be proportional to the increase in wall shear stress, resulting in the need of high extrusion pressure. In the higher weight fractions (over 40 wt %) of alginate composition in the composite, the extrusion pressure went beyond the limitations of our equipment; therefore, we used a weight fraction of alginate in the composite to less than 40 wt %.

The strut diameter in a layer-by-layered structure affects both the mechanical properties and activities of seeded cells, because the struts can constitute various pore structures (pore size, porosity, and tortuosity).[34,35] For this reason, the controllability of strut diameter is an important processing parameter. To observe the effects of processing factors on strut diameter for various compositions of alginate in the composite, the dependency on the applied pressure, temperature, and nozzle speed was determined. Figure 2a−c shows the effects of the processing parameters (applied pressure ($P$), temperature (T), and nozzle moving speed (MS), respectively) on the final strut diameter for the various PCL: alginate ratios. As shown in Figure 2 (a,b), with increasing pressure and temperature in the process, all PCL/alginate composite strut diameters increased. However, with an increased weight fraction of alginate under constant $P$ and $T$, the strut diameter of composites was reduced significantly, because the dispersed alginate in the composite results in dispersion of stored elastic deformation energy and obstruction of the elastic recovery of deformed PCL/alginate-mixture within the nozzle. Additionally, with increasing nozzle speed, the strut size decreased (Figure 2c). On the basis of these results, to obtain a homogeneous strut diameter, we used various extrusion pressures and temperatures, but maintained a constant nozzle speed, 5 mm/s. The processing conditions for composite fabrication are described in Table 1.

**Pore Structure Analysis.** Using these processing conditions, we fabricated four different composite scaffolds: pure PCL and PCL/alginate composites (10, 20, and 30 wt % of alginate). Figure 2d−g show optical and SEM images of PP and various PAs (PA-10, PA-20, PA-30). As shown in the optical images, with an increasing alginate weight fraction, the color of the composite changed gradually from white to pale yellow. As shown in the surface and cross-sectional SEM images, the struts of the PP and PAs showed similar diameters, and the struts of each layer were well offset from the previous layer (100% offset). Offset scaffolds in multilayered structures can evoke enhanced bioactive properties, including higher cell seeding efficiency, cell viability, and calcium deposition due to effective contact between the cells and osteogenic fluid.[33,36]

As seen in the SEM images, the pure PCL (PP) showed a smooth surface and regular microinternal pores, while for the composites (PAs), the strut surface was highly roughened, because the embedded alginate swelled during the cross-linking process. Qualitatively, as the alginate content of the composite increased, more highly roughened surfaces were observed.

Pore structure, including strut size, in multilayered structure is an important design parameter, because it affects both the mechanical properties and cellular responses (seeding efficiency, cell-migration, and growth). To regenerate bone, because the pore size for microsized struts has been suggested to be 100−400 $\mu$m,[37] the penetrating pore size, defined in the cross-sectional SEM image of Figure 2d, of the PP and PAs was set at 150 $\mu$m. Table 2 shows the measured apparent and penetrating pore sizes and the strut diameters of PP and PA composite scaffolds. The penetrating pore size of the scaffolds was 130−160 $\mu$m. Although the pore size did not completely match the initially designed value, the range was reasonable. Because of the similar strut diameter and pore size of the scaffolds, the porosity was also similar, at 71−75%. Therefore, the structural analysis indicates that the scaffolds have similar microinternal architectures.

**Surface Roughness.** Along with the interior pore structure of scaffolds, their surface topography also influences protein absorption and biological activity, such as initial cell attachment, cell migration, cell growth, modulation of phenotypic differentiation, and responses to extracellular signals.[38,39] In particular, for hard tissue regeneration, a titanium substrate roughened at the micro- and submicron scales significantly induced osteo-integration by improving MG63 differentiation and local factor production.[40] Also, a surface roughened with nanosized patterns induced a variety of biological signals promoting integrin-meditated adhesion, actin cytoskeleton organization, and even selective modulation of osteogenic differentiation.[41−44]

**Table 2. Strut Diameters and Pore Structures (Pore Size and Porosity) of PP and PA-Composite Scaffolds**

| | PP | PA-10 | PA-20 | PA-30 |
|---|---|---|---|---|
| strut diameter ($\mu$m) | 343.2 ± 55.2 | 362.1 ± 29.8 | 346.5 ± 24.0 | 354.6 ± 21.1 |
| apparent pore size ($\mu$m) | 610.6 ± 52.5 | 621.4 ± 31.7 | 651.1 ± 38.2 | 640.3 ± 24.0 |
| penetrating pore size ($\mu$m) | 131.6 ± 46.5 | 133.2 ± 38.8 | 147.1 ± 43.3 | 159.2 ± 30.0 |
| porosity (%) | 71.6 ± 1.1 | 73.8 ± 0.4 | 74.7 ± 0.4 | 75.2 ± 0.4 |



DOI: 10.1021/co500033h
ACS Comb. Sci. 2015, 17, 87−99

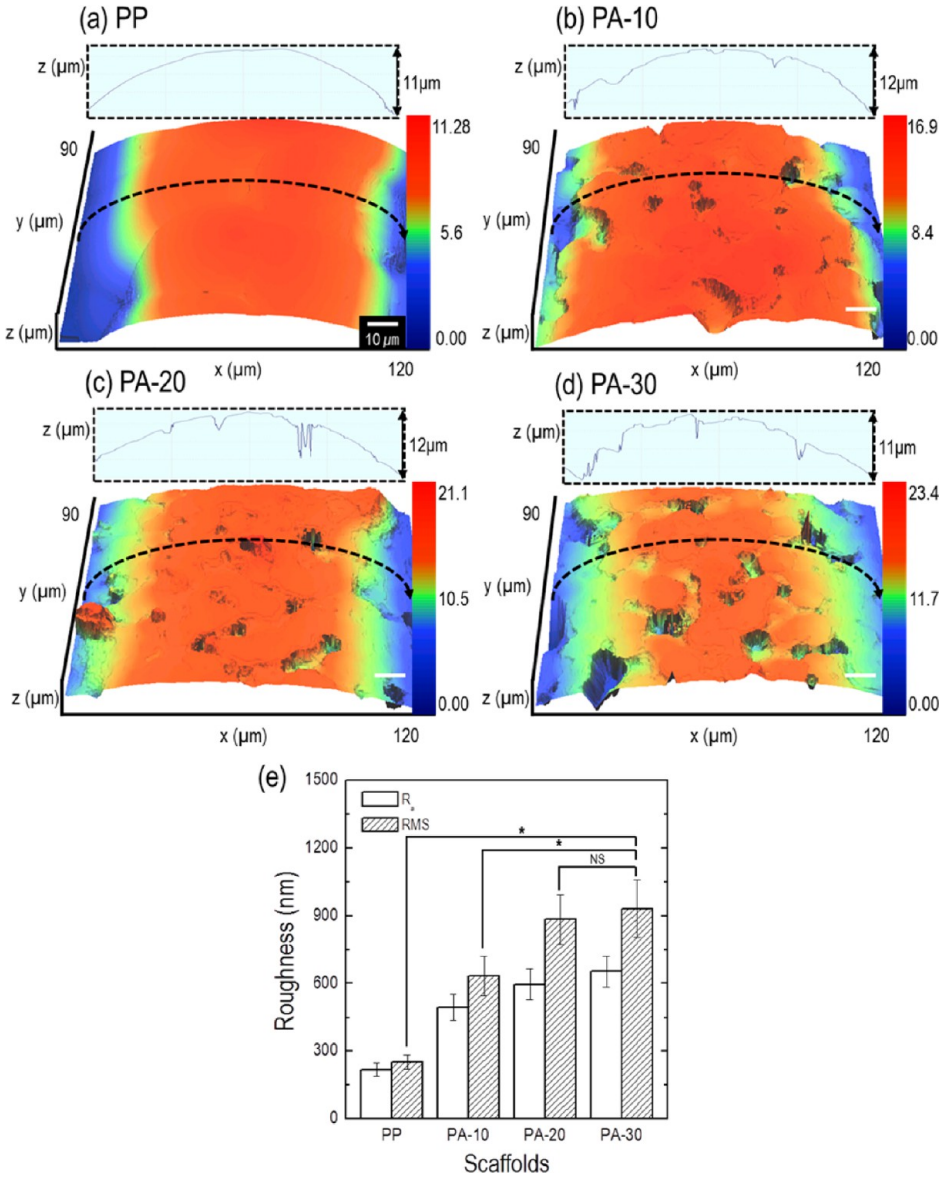


**Figure 3.** Three-dimensional topography of the strut surfaces of (a) pure PCL, (b) PA-10, (c) PA-20, and (d) PA-30 scaffolds, and (e) the $R_a$ and RMS (root-mean-square) values of the surfaces. *$p < 0.05$ and NS indicate a significant difference and nonsignificance, respectively.

**Table 3. Surface Roughness Values ($R_a$, RMS, and $R_t$) of the Scaffolds**

| | PP | PA-10 | PA-20 | PA-30 |
|---|---|---|---|---|
| $R_a$ (nm) | 218.7 ± 30.0 | 494.5 ± 113.0 | 575.4 ± 147.7 | 653.5 ± 137.1 |
| RMS (nm) | 252.8 ± 30.5 | 633.1 ± 174.9 | 885.1 ± 221.0 | 932.7 ± 254.8 |
| $R_t$ ($\mu$m) | 1.0 ± 0.1 | 3.2 ± 0.4 | 4.7 ± 0.6 | 5.4 ± 0.6 |

Figure 3a–d shows three-dimensional roughness images of the PP and PA composite scaffolds (PA-10, PA-20, PA-30), respectively. To evaluate roughness quantitatively, various values were acquired using the roughness curves in Figures 3a–d. The average roughness ($R_a$) was obtained using the equation, $R_a = (\int |f(x)| dx)/L$, where $L$ is the length of the measuring line and $f(x)$ represents a roughness curve in the $z$-direction. Also, the maximum roughness height, $R_t = R_H - R_L$, was measured using the highest value ($R_H$) and lowest value ($R_L$). In Table 3, the roughness values ($R_a$, RMS, and $R_t$) are described. As shown in Figure 3e, the roughness of the composite scaffolds increased gradually with increasing composite alginate content. This phenomenon was coincident with the surface SEM images of the composites, because the alginate component dispersed on the surface layer in the struts swelled during the cross-linking process. The optimized surface roughness for regenerating bone tissues has been debated, because it depends on the cell type, pattern shape, and the stiffness of the patterned surface; however, specific ranges for bone tissue regeneration have been recommended. According to Kubo et al., hierarchical micro/nanohybrid $TiO_2$ surfaces having ranges of 0.5–1.5 $\mu$m and 100–500 nm can induce substantial ALP activity, gene expression, and calcium deposition relative to pure microsized structures.[45] Also, to obtain rapid osteo-integration of osteoblast-like cloned mouse cells (MC3T3-E1), a surface roughness ($R_a$) of 810 nm was



DOI: 10.1021/co500033h
ACS Comb. Sci. 2015, 17, 87–99

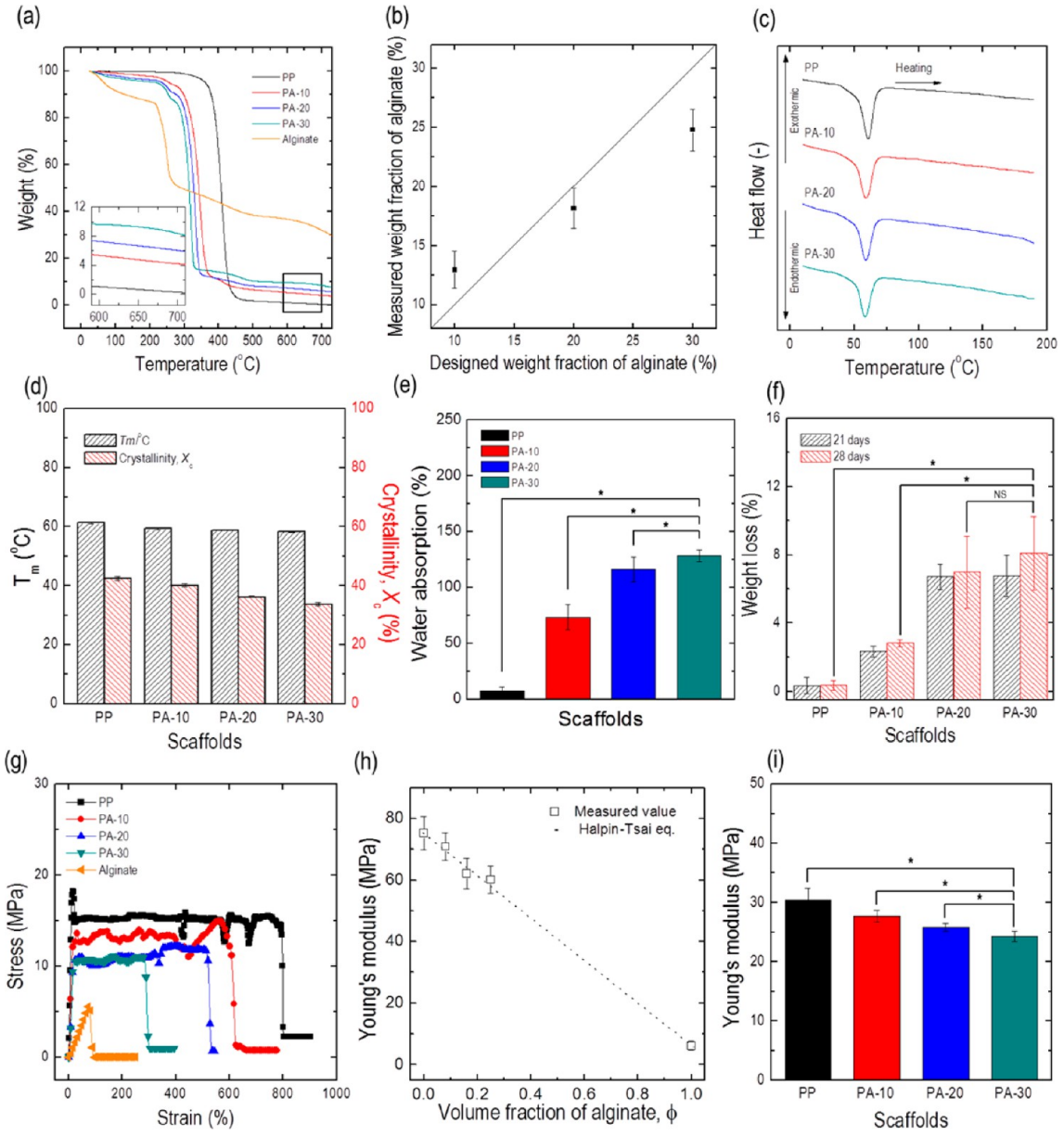


**Figure 4.** (a) Thermogravimetric (TGA) analysis of PP and PA-composites. (b) Comparison of the designed alginate weight fraction in the composite and the measured weight fraction determined from the TGA data at 600 °C. (c) DSC results for PP and PA-composites, and (d) melting temperature ($T_m$) and crystallinity (%). (e) Comparison of water absorption of PP and PA-composite scaffolds. (f) Weight loss of PP and PA-composite scaffolds in PBS for two time periods (21 and 28 days). (g) Stress−strain curves for PP and PA-composite struts and (h) Young's moduli. (i) Young's moduli for PP and PA-composite scaffolds. *$p < 0.05$ and NS indicate a significant difference and nonsignificance, respectively.

**Table 4. Mechanical Properties of PP and PA-Composite Scaffolds**

| | PP | PA-10 | PA-20 | PA-30 |
|---|---|---|---|---|
| max. tensile strength (MPa) | 3.7 ± 0.2 | 2.8 ± 0.2 | 2.7 ± 0.1 | 2.6 ± 0.1 |
| max. tensile strain (%) | 63.3 ± 10.1 | 45.6 ± 8.8 | 37.7 ± 12.4 | 30.3 ± 4.0 |
| Young's modulus (MPa) | 30.5 ± 2.0 | 27.7 ± 1.0 | 25.8 ± 0.6 | 24.3 ± 0.9 |

recommended.[46] Recently, we found that cell (MG63)-imprinted surfaces, which have a roughness, $R_a$ = 702 ± 87 nm, showed reasonable ALP activity and calcium deposition with MG63.[42] Therefore, the PA-30 scaffold, which has a roughness of $R_a$ = 653.5 ± 68.1 nm, may induce cell responses, proliferation, and differentiation.

**Thermogravimetric Analysis (TGA).** Figure 4a show the TGA graphs obtained from the thermograms of the pure PCL, PA composites (10, 20, 30 wt % of alginate), and pure alginate. As shown in Figure 4a, the TGA data for pure alginate showed that degradation began at 30 °C, and that for the composites, the degradation temperature was dependent on the alginate weight fraction. Using the degradation curves, we can compare the alginate concentration in the theoretical weight fraction in the composites with the actual amount in the fabricated composites. As shown in Figure 4b, the designed alginate content of the composites correlated well with the concentration in the PCL/alginate composites determined experimentally.



DOI: 10.1021/co500033h
ACS Comb. Sci. 2015, 17, 87−99

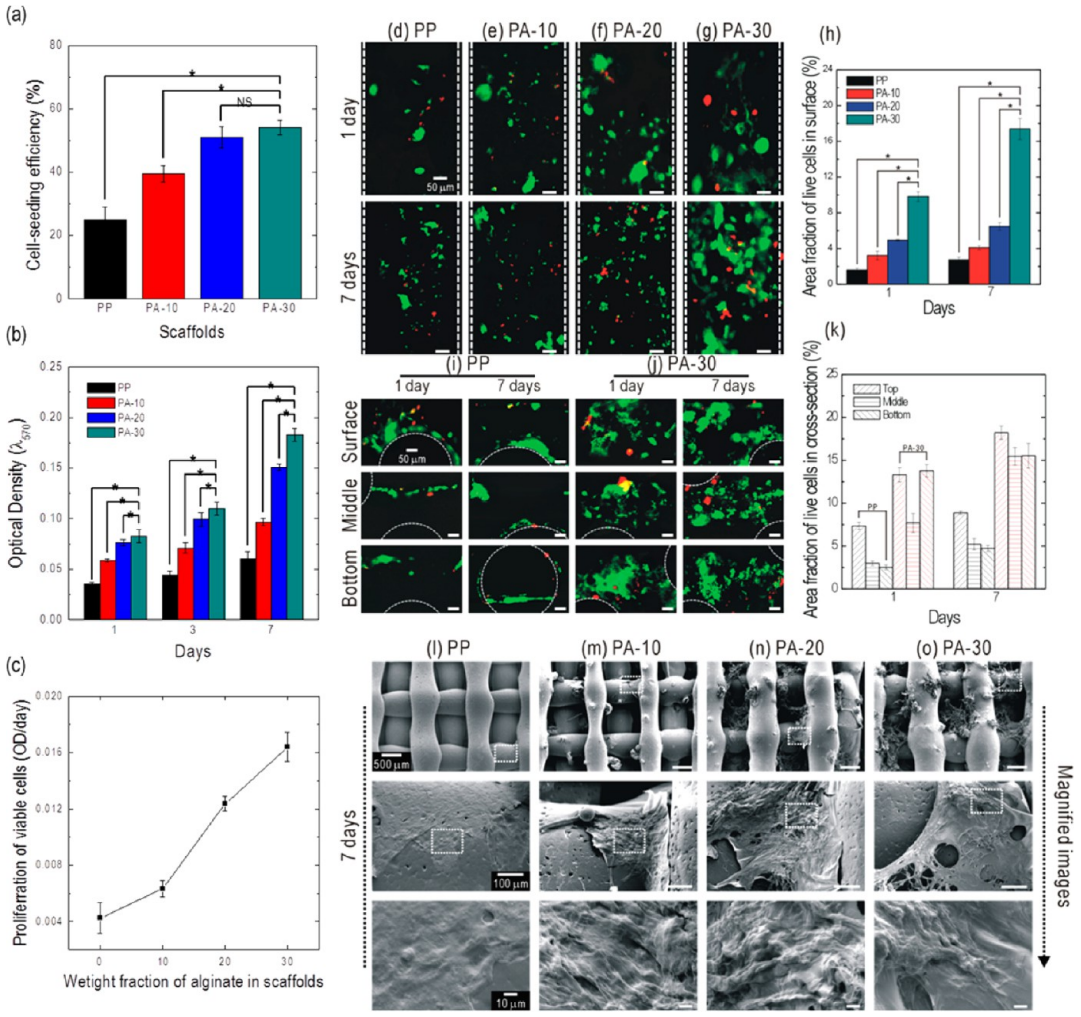


**Figure 5.** (a) Cell-seeding efficiencies for the PP and PA-composite scaffolds after culture for 12 h. (b) Cell viability (optical density) at 1, 3, and 7 days, as indicated by MTT assay of MC3T3-E1 cells seeded onto the PP and PA-composite scaffolds. (c) Proliferation of viable cells, defined as the slope of the MTT results. Live (green) MC3T3-E1 cells after 1 and 7 days of culture on (d) PP, (e) PA-10, (f) PA-20, and (g) PA-30 scaffolds. (h) Area fraction of live cells on scaffold surfaces. Images of (i) PP and (j) PA-30 scaffolds cultured for 1 and 7 days showing the cell distribution the surface, middle, and bottom layers. Cells in each layer were enumerated using ImageJ, and (k) the distribution of cells was calculated from the number of each layer. (l–o) SEM micrographs of cell morphology for PP and various composite scaffolds after culturing 7 days. *$p < 0.05$ and NS indicate a significant difference and nonsignificance, respectively.

**DSC Results.** Figure 4c shows DSC results of the pure PCL (PP) and various composites (PA-10, PA-20, PA-30, respectively). The melting point ($T_m$) and degree of crystallinity ($X_c$) of the composites had a tendency to decrease with increasing alginate weight fraction (Figure 4d). The degrees of crystallinity of pure PCL and PA-30 were calculated as 42.5% and 33.7%, assuming that the enthalpy of 100% crystalline PCL is 166 J $g^{-1}$.[47] These phenomena can be attributed to the hydrogen bond interactions between the carbonyl groups of the PCL and the OH groups in the alginate. Such interactions occur in the amorphous region, thus overwhelming the crystallization of the PCL. From the degree of crystallinity analysis, we can estimate that the mechanical properties of the composites may be degraded slightly due to hindrance by the alginate component of the crystallization mobility of the PCL molecules versus that of pure PCL. However, the mechanical properties do not correlate completely with the degree of crystallinity of the materials.[48]

**Water Absorption (WA) and Biodegradability.** Water absorption (WA) by the scaffolds reflects the absorption of body fluids and the effective transfer of cell nutrients and metabolites. Figure 4e displays the water absorption of PP and PA composite scaffolds. The WA of the composite scaffolds was significantly higher than that of the pure PCL scaffold; indeed, the WA of the PA-30 scaffold was 12-fold greater than that of pure PCL, because of the hydrophilic properties of the dispersed alginate.

To evaluate scaffold biodegradability, the weight loss (%) of the scaffolds over 21 and 28 days was measured in PBS at 37 °C (Figure 4f). For pure PCL (PP), the weight loss (%) over 28 days was negligible, while that of the composite scaffolds was higher. In particular, the weight loss of PA-30 was 8% on day 28. This indicates that the degradation of composite scaffolds was dependent on the alginate component, and that despite its cross-linking, the embedded alginate in the composite degraded gradually.

**Tensile Test of Single Struts and Scaffolds.** Appropriate mechanical properties of biomedical scaffolds are required for regeneration of various tissues, because sufficient mechanical strength supports new tissue formation and sustains its physical


DOI: 10.1021/co500033h
ACS Comb. Sci. 2015, 17, 87–99

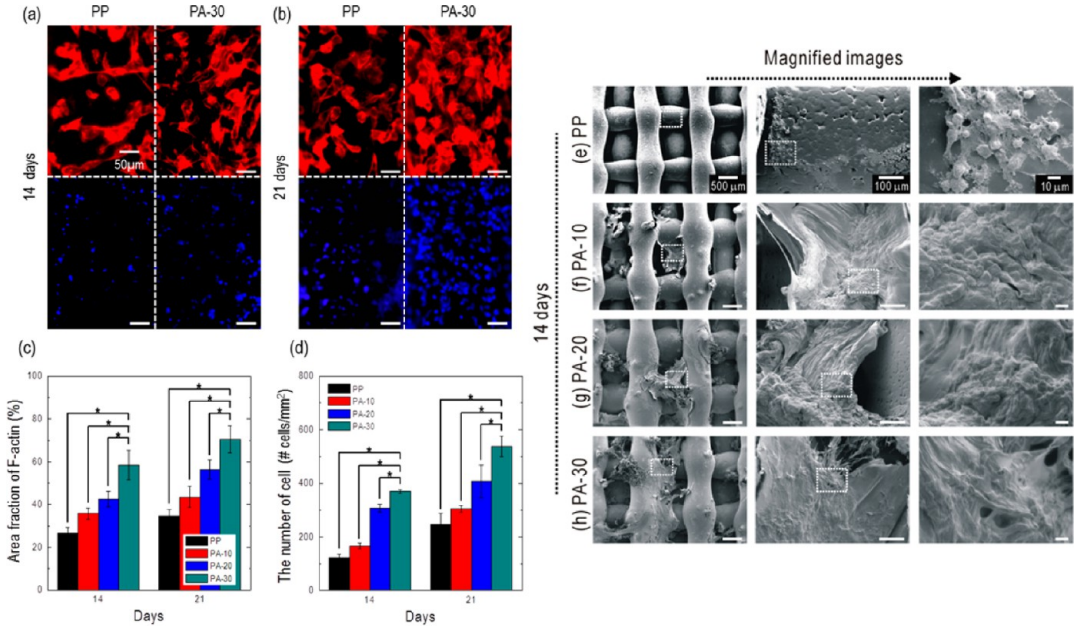


**Figure 6.** DAPI (green) and phalloidin images after culture for 14 and 21 days on (a) PP and (b) PA-30 scaffolds. (c) Area fraction of F-actin and (d) number of cells on PP and PA-composite scaffolds. SEM micrographs of cell morphology for (e) PP and (f–h) composite scaffolds after culturing 14 days.

shape and structure. Scaffolds need highly porous structures to achieve good biological interactions between cells and substrates; however, the mechanical stability of porous scaffolds can be reduced significantly. From this reason, appropriately balanced mechanical properties and pore structures must be achieved. Alginates are reasonably biocompatible polymers, but poor mechanical properties have been an obstacle to their use in scaffolds for hard tissue regeneration. However, composite alginate-based PCL scaffolds can have improved mechanical properties relative to those of pure alginate scaffolds.

To assess the mechanical properties of pure PCL and the composites, we conducted a tensile test using a single strut (diameter = 357 ± 31 $\mu$m) in a wet state. Figure 4g shows the typical stress–strain curves for a single strut of PP and composites (PA-10, PA-20, PA-30) at a constant stretching velocity of 2 mm/s. The pure PCL strut showed the highest modulus ($E_p$, 75.2 ± 5.4 MPa) and break strain (670.8 ± 85.2%), while the composite struts showed gradually decreasing moduli; lowest value was for the PA-30 strut ($E_a$, 60.1 ± 4.5 MPa), which had the highest alginate volume fraction, which has a low modulus, 6.2 ± 1.5 MPa. The Young's modulus of the composite ($E_c$) was analyzed using the following modified Halpin–Tsai equation:[49]

$$E_c = 0.375\frac{1 + \alpha\beta_L\varphi_a}{1 - 2\beta_L\varphi_a} \times E_p + 0.625\frac{1 + 2\beta_W\varphi_a}{1 - 2\beta_W\varphi_a} \times E_p$$

$$\beta_L = \frac{\Lambda_{ap} - 1}{\Lambda_{ap} + \alpha}$$

$$\beta_W = \frac{\Lambda_{ap} - 1}{\Lambda_{ap} + 2}$$

where $E_c$ and $\phi_a$ are the Young's moduli of the composite and the volume fraction of alginate in the composite, and $\Lambda_{ap} = E_a/E_p$, respectively. The parameter ($\alpha$) is dependent on the geometry and boundary conditions of the alginate in the mixture. According to Halpin,[49] the parameter can be expressed as

$$\alpha = \frac{W + L}{t}$$

In the relationship, $W$, $L$, and $t$ are the average length, width, and thickness of the alginate. In this work, we assumed that the alginate in the mixture was of a square shape, so that the value was 2. Figure 4h shows a comparison of the calculated and measured moduli. The measured modulus of the composite followed the Halpin–Tsai equation well. Therefore, the modulus of the composites was dependent on the volume fraction of the alginate composition, and mechanical controllability of the composite scaffolds would be feasible if the alginate volume fraction can be changed.

To assess the mechanical properties of the pure PCL and PA composite scaffolds, tensile testing was performed in a wet state (Figure 4i). The Young's moduli of the composite scaffolds ranged from 24 to 31 MPa. These results showed a similar tendency to those of tensile tests of single struts. The measured Young's modulus was lower than that of human trabecular bone (50–100 MPa).[50] However, the modulus ($E_{cs}$) of the porous composite scaffold can be altered by varying the porosity ($\varphi$) according to the following equation:[51]

$$E_{cs} = E_o \times (1 - \varphi^{2/3})$$

$E_o$ is the Young's modulus of the pore-free sample. Although the Young's modulus cannot be made identical to that of human trabecular bone, it is controllable to some extent by manipulating the porosity of the composite scaffold. The mechanical properties of single struts and scaffolds are shown in Table 4.

**Cell-Seeding Efficiency and Viability.** Cell-seeding efficiency can significantly affect initial cell attachment and tissue regeneration and is highly dependent on the chemical composition, micro/nanotopographical structure, and pore structure, including pore size, strut size, and tortuosity.[33]



DOI: 10.1021/co500033h
ACS Comb. Sci. 2015, 17, 87–99

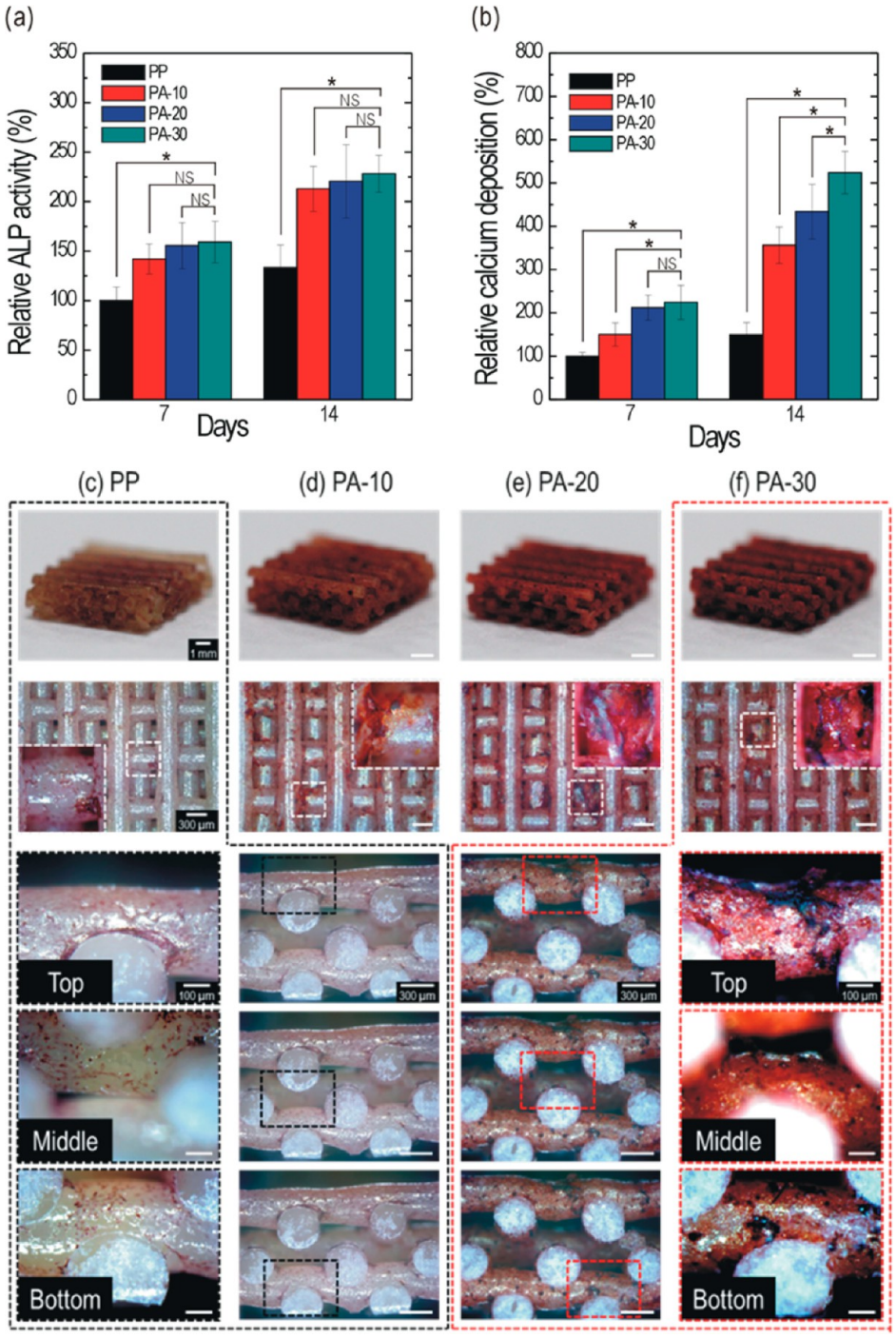


**Figure 7.** (a) Relative alkaline phosphatase (ALP) activities and (b) relative levels of calcium deposition on composite scaffolds with various alginate weight fractions from 7 to 14 days. (c–f) 3D shape and cross-sectional optical images of ARS staining of the scaffolds after 14 days of culture. *$p$ < 0.05 and NS indicate a significant difference and nonsignificance, respectively.

**Table 5. Total Protein Contents of PP and PA-Composite Scaffolds after 7 and 14 Days of Culture**

| | BCA [mg] | | | |
|---|---|---|---|---|
| | PP | PA-10 | PA-20 | PA-30 |
| 7 days | 26.1 ± 3.1 | 44.3 ± 5.0 | 51.6 ± 4.8 | 62.8 ± 12.8 |
| 14 days | 51.3 ± 10.7 | 62.5 ± 4.7 | 73.4 ± 7.4 | 76.7 ± 4.6 |

Figure 5a shows the cell-seeding efficiency of the PP and PA composite scaffolds. The cell-seeding efficiency (CSE) of the pure PCL scaffold was 24.9 ± 4.1%, while that of the PA composite scaffolds increased gradually from 39.4 ± 2.7% for PA-10 to 54.1 ± 2.3% for PA-30. This was likely attributable to the good wetting ability and higher water absorption of the composite scaffolds versus the pure PCL scaffold. Similar attributes of alginate in various biocomposites have been well described in the previous studies.[52,53]

Figure 5b shows the viability of preosteoblast cells (MC3T3-E1) cultured on the PP and PA composite scaffolds, as determined by MTT assay. The optical density (OD) of the composite scaffolds was significantly higher than that of the pure PCL scaffold ($p$ < 0.05) for all culture periods (1, 3, and 7



DOI: 10.1021/co500033h
ACS Comb. Sci. 2015, 17, 87–99

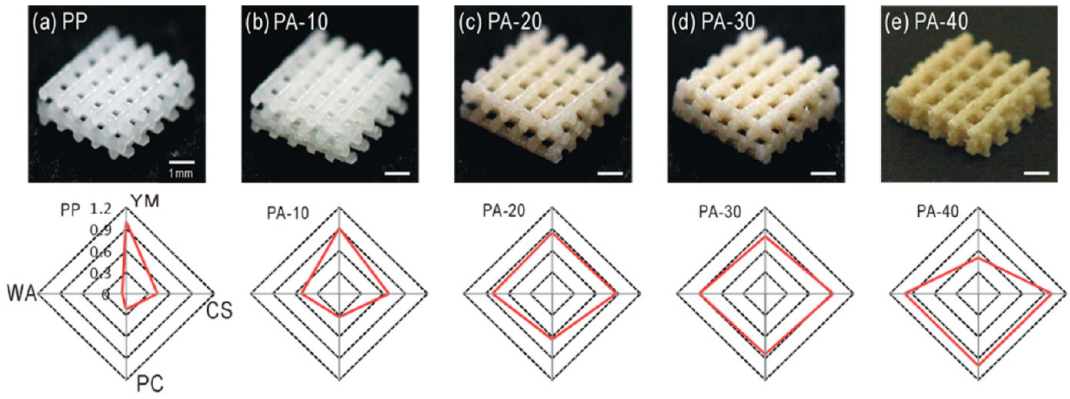


| | (a)PP | (b)PA-10 | (c)PA-20 | (d)PA-30 | (e)PA-40 |
|---|---|---|---|---|---|
| Young`s modulus(YM) (MPa) | 30.6 ± 2.0 | 27.7 ± 1.0 | 25.8 ± 0.6 | 24.3 ± 0.9 | 15.2 ± 1.3 |
| Cell seeding efficiency(CS) (%) | 24.9 ± 4.1 | 39.4 ± 2.7 | 51.0 ± 3.3 | 54.1 ± 2.3 | 58.6 ± 3.6 |
| proliferation of viable cells(PC) (OD/day) | 0.004 ± 0.001 | 0.006 ± 0.001 | 0.012 ± 0.001 | 0.016 ± 0.001 | 0.019 ± 0.004 |
| Water absorption(WA) (%) | 7.6 ± 3.3 | 73.4 ± 11.4 | 116.4 ± 10.8 | 128.5 ± 5.2 | 143.5 ± 8.6 |

**Figure 8.** Optical images and radial graphs showing normalized physical and in vitro cellular activities for (a) PP and (b–e) various composite scaffolds.

days). Moreover, with increasing alginate content, the number of viable cells increased, indicating that the dispersed alginate in the composite scaffolds plays an important role in cell proliferation. The rate of increase in viable cell number was determined from the slope of the OD and the time period. Figure 5c shows the rates of increase in viable cell numbers in pure PCL and the various composite scaffolds. With an increasing alginate weight fraction, cell proliferation increased significantly.

Figure 5d–g shows fluorescence images of the strut surface (PP, PA-10, PA-20, PA-30, respectively) at 1 and 7 days, in which live cells are green. In the images, the number of live cells cultured in the composite scaffolds was larger than that of the PP scaffolds. In particular, for the PA-30 composite scaffold, the attached cells showed a well-developed stretching shape as compared to cells on the other scaffolds (Figure 5h).

Figure 5i, j shows the cell distribution in the top, middle, and bottom regions of the pure PCL and PA-30 composite scaffolds. Cells in the composite scaffold (PA-30) were distributed more homogeneously than those in the PP scaffold on culture days 1 and 7. In Figure 5k, the cell distribution among the regions based on the number of live cells is shown. To observe the morphology of the cells on the PP and composite scaffolds, SEM images were obtained after 7 days of cell culture, as shown in Figure 5l–o. The preosteoblasts were found to be well proliferated on the strut surfaces as well as in the pores of the composite scaffolds compared to the PP scaffold.

Figure 6a, b shows fluorescence images after 14 and 21 days of culture for the PP and PA-30 composite scaffold. Nuclei and F-actin are shown in blue and red, respectively. Cells in both scaffolds were well proliferated, but for the PA-30, the cells were more actively grown. Figure 6c, d shows the measured F-actin area and number of nuclei for the PP and PA scaffolds, and Figure 6e–h displays the SEM images of the proliferated cells on the PP and composite scaffolds after 14 days of cell culture. With an increasing alginate weight fraction in the composite scaffolds, the cells were well proliferated.

**ALP Activity and Calcium Mineralization.** Figure 7a and b shows the ALP activity and alizarin red-S staining (ARS), respectively, after cell culture for 7 and 14 days, normalized to the total protein content (Table 5). ALP and ARS data were normalized to those of the pure PCL scaffold. The composite scaffolds showed greater ALP activities than the pure PCL scaffold. Also, ALP activity increased in proportion with the increasing alginate weight fraction.

Alizarin red-S (ARS) was used to determine the level of differentiation of cells. The ARS intensities of the composite scaffolds were greatly improved versus that of the pure PCL scaffold, and increased gradually with increasing alginate weight fraction. Therefore, the composite scaffolds supplemented with alginate could facilitate osteogenic differentiation, as indicated by the increased ALP activity and mineralized extracellular matrix deposition.

Figure 7c–f shows optical images of ARS staining of the pure PCL and composite scaffolds at 14 days of cell culture. Red coloration indicates areas of calcium deposition; the red coloration density increased with increasing alginate weight fraction. Magnified images of pure PCL and PA-30 scaffolds indicated a different red coloration of the surface and top, middle, and bottom regions.

**Optimal Composition of an Alginate in PA Scaffolds.** To assess the optimum composition of an alginate in the PA scaffolds, we used four different PCL/alginate composite scaffolds and four different quantities representing physical and in vitro cellular activities (tensile modulus of single strut, YM; water absorption, WA; cell seeding efficiency, CS; and proliferation rate of viable cells, PC). Figure 8a–e shows the optical images and evaluating values of the composite scaffolds. The composite scaffolds consisting of various alginate weight fractions (10, 20, 30, and 40 wt %) exhibited well-defined pore structures, which consisted of multilayered microsized struts. In the radial graphs of Figure 8a–e, the quantitative values were normalized with the each maximum value, which was shown in the table of Figure 8. As shown in the Results, although the tensile modulus of PA scaffolds was decreased by ~49%


DOI: 10.1021/co500033h
ACS Comb. Sci. 2015, 17, 87–99

compared with the pure PCL scaffold (PP), significantly improved water absorption and biological activities were observed. In addition, regarding the aspect of optimum composition of alginate in the PA scaffolds, the PA-40 scaffold (40 wt % of alginate in PCL) showed the significantly improved cellular activities versus those of other PA scaffolds, but drastic decrease (about ∼49%) of the tensile modulus was observed. On the basis of these simple evaluations using the physical and in vitro biological results, we can carefully suggest that the PA-30 scaffold (30 wt % of alginate) can be the most optimum value of alginate composition of the PA scaffolds in aspects of the reasonable mechanical properties and cellular responses compared to any other PA-scaffolds.

## ■ CONCLUSIONS

In this study, to enhance the biological activities of the synthetic polymer PCL and to improve the mechanical properties of alginates, PCL/alginate-based composite scaffolds were prepared. The PCL/alginate composite scaffolds, consisting of various alginate weight fractions (10, 20, and 30 wt %), exhibited well-defined pore structures, which consisted of multilayered microsized struts. Although the Young's modulus of PA scaffolds was decreased compared with the pure PCL scaffold, significantly improved water absorption and wetting behavior were observed. Regarding biological aspects, preosteoblast (MC3T3-E1) cells were cultured on the composite scaffolds comprising various alginate weight fractions. The cell-seeding efficiency and cell viability were markedly improved versus those of the pure PCL scaffold. ALP and mineralization assays revealed that PA scaffolds significantly induced cell differentiation compared to the pure PCL scaffold, which was confirmed quantitatively through optical imaging of ARS staining after culture for 14 days. On the basis of these physical and in vitro biological results, we suggest that PCL/alginate composite scaffolds may have potential for use in scaffolds for hard tissue regeneration.

## ■ AUTHOR INFORMATION

### Corresponding Author

*E-mail: xrdghk@gmail.com. Tel: +82-31-290-7828.

### Notes

The authors declare no competing financial interest.

## ■ ACKNOWLEDGMENTS

This research was financially supported by the National Research Foundation of Korea grant funded by the Ministry of Education, Science, and Technology (MEST) (Grant NRF-2012R1A2A2A01017435) and also was partially supported by a grant of the Korean Health Technology R&D Project, Ministry of Health & Welfare, Republic of Korea (Grant A120942).

## ■ REFERENCES

(1) Wahl, D. A.; Czernuszka, J. T. Collagen−hydroxyapatite composites for hard tissue repair. *Eur. Cells Mater.* **2006**, *11*, 43−56.
(2) Hollister, S. J. Porous scaffold design for tissue engineering. *Nat. Mater.* **2005**, *4*, 518−524.
(3) Hutmacher, D. W. Scaffolds in tissue engineering bone and cartilage. *Biomaterials* **2000**, *21*, 2529−2543.
(4) Freed, L. E.; Vunjak-Novakovic, G.; Biron, R. J.; Eagles, D. B.; Lesnoy, D. C.; Barlow, S. K.; Langer, R. Biodegradable polymer scaffolds for tissue engineering. *Nat. Biotechnol.* **1994**, *12*, 689−693.
(5) Zhang, R.; Ma, P.X. J. Poly(α-hydroxyl acids)/hydroxyapatite porous composites for bone-tissue engineering. I. Preparation and morphology. *J. Biomed. Mater. Res.* **1999**, *44*, 446−455.
(6) Yang, S.; Leong, K. F.; Du, Z.; Chua, C. K. The design of scaffolds for use in tissue engineering. Part I. Traditional factors. *Tissue Eng.* **2001**, *7*, 679.
(7) Du, Y.; Ghodousi, M.; Qi, H.; Haas, N.; Xiao, W.; Khademhosseini, A. A. Sequential assembly of cell laden hydrogel Constructs to engineer vascular-Like microchannels. *Biotechnol. Bioeng.* **2011**, *108*, 1693−1703.
(8) Ji, W.; Sun, Y.; Yang, F.; van den Beucken, J. J. J. P.; Fan, M.; Chen, Z.; Jansen, J. A. Bioactive electrospun scaffolds delivering growth factors and genes for tissue engineering applications. *Pharm. Res.* **2011**, *28*, 1259−1272.
(9) Janicki, P.; Schmidmaier, G. What should be the characteristics of the ideal bone graft substitute? Combining scaffolds with growth factors or stem cells. *Injury* **2011**, *42*, S77−S81.
(10) Luo, Y.; Lode, A.; Gelinsky, M. Direct plotting of three-dimensional hollow fiber scaffolds based on concentrated alginate pastes for tissue engineering. *Adv. Healthcare Mater.* **2012**, *2*, 777−783.
(11) Sachlos, E.; Czernuszka, J. T. Making tissue engineering scaffolds work. Review on the application of solid freeform fabrication technology to the production of tissue engineering scaffolds. *Eur. Cell Mater.* **2003**, *5*, 29−39.
(12) Billiet, T.; Vandenhaute, M.; Schelfhout, J.; Vlierberghe, S. V.; Dubruel, P. A review of trends and limitations in hydrogel-rapid prototyping for tissue engineering. *Biomaterials* **2012**, *33*, 6020−6041.
(13) Leong, K. F.; Cheah, C. M.; Chua, C. K. Solid freeform fabrication of three-dimensional scaffolds for engineering replacement tissues and organs. *Biomaterials* **2003**, *24*, 2363−2378.
(14) Hoque, M. E.; Chuan, Y. L.; Pashby, I. Extrusion based rapid prototyping technique: An advanced platform for tissue engineering scaffold fabrication. *Biopolymers* **2013**, *97*, 83−93.
(15) Jang, C. H.; Cho, Y. B.; Yeo, M. G.; Kim, G. H. Mastoid Obliteration Using Three-Dimensional Composite Scaffolds Consisting of Polycaprolactone/β-Tricalcium Phosphate/Collagen Nanofibers: An In Vitro and In Vivo Study. *Macromol. Biosci.* **2013**, *13*, 660−668.
(16) Jin, G. H.; Kim, G. H. The effect of sinusoidal AC electric stimulation of 3D PCL/CNT and PCL/β-TCP based bio-composites on cellular activities for bone tissue regeneration. *J. Mater. Chem. B* **2013**, *1*, 1439−1452.
(17) Li, M. G.; Tian, X. Y.; Chen, X. B. A brief review of dispensing-based rapid prototyping techniques in tissue scaffold fabrication: role of modeling on scaffold properties prediction. *Biofabrication* **2009**, *1*, 032001.
(18) Son, J. G.; Kim, G. H. Three-dimensional plotter technology for fabricating polymeric scaffolds with microgrooved surfaces. *J. Biomater. Sci., Polym. Ed.* **2009**, *20*, 2089−2101.
(19) Babensee, J. E.; Cornelius, R. M.; Brash, J. L.; Sefton, M. V. Immunoblot analysis of proteins associated with HEMA−MMA microcapsules: Human serum proteins in vitro and rat proteins following implantation. *Biomaterials* **1998**, *19*, 839−849.
(20) Porter, R. M.; Akers, R. M.; Howard, R. D.; Forsten-Williams, K. Alginate encapsulation impacts the insulin-like growth factor-I system of monolayer-expanded equine articular chondrocytes and cell response to interleukin-1β. *Tissue Eng.* **2007**, *13*, 1333−1345.
(21) Costa-Pinto, A. R.; Correlo, V. M.; Sol, P. C.; Bhattacharya, M.; Charbord, P.; Delorme, B.; Reis, R. L.; Neves, N. M. Osteogenic differentiation of human bone marrow mesenchymal stem cells seeded on melt based chitosan scaffolds for bone tissue engineering applications. *Biomacromolecules* **2009**, *10*, 2067−2073.
(22) Cohen, D. L.; Malone, E.; Lipson, H.; Bonassar, L. J. Direct freeform fabrication of seeded hydrogels in arbitrary geometries. *Tissue Eng.* **2006**, *12*, 1325−1335.
(23) Ahn, S. H.; Lee, H. J.; Puetzer, J.; Bonassar, L. J.; Kim, G. H. Fabrication of cell-laden three-dimensional alginate-scaffolds with an aerosol cross-linking process. *J. Mater. Chem.* **2012**, *22*, 18735−18740.


DOI: 10.1021/co500033h
*ACS Comb. Sci.* 2015, 17, 87−99

(24) Luo, Y.; Wu, C.; Lode, A.; Gelinsky, M. Hierarchical mesoporous bioactive glass/alginate composite scaffolds fabricated by three-dimensional plotting for bone tissue engineering. *Biofabrication* **2013**, *5*, No. 015005.
(25) Lin, H. R.; Yeh, Y. J. Porous alginate/hydroxyapatite composite scaffolds for bone tissue engineering: Preparation, characterization, and in vitro studies. *J. Biomed. Mater. Res., Part B* **2004**, *71B*, 52−65.
(26) Liu, X.; Ma, P. X. Polymeric scaffolds for bone tissue engineering. *Ann. Biomed. Eng.* **2004**, *32*, 477−486.
(27) Luo, Y.; Lode, A.; Sonntag, F.; Nies, B.; Gelinsky, M. Well-ordered biphasic calcium phosphate−alginate scaffolds fabricated by multi-channel 3D plotting under mild conditions. *J. Mater. Chem. B* **2013**, *1*, 4088−4098.
(28) Kim, Y. B.; Kim, G. H. Collagen/alginate scaffolds comprising core (PCL)−shell (collagen/alginate) struts for hard tissue regeneration: fabrication, characterisation, and cellular activities. *J. Mater. Chem. B* **2013**, *1*, 3185−3194.
(29) Lee, H. J.; Ahn, S. H.; Bonassar, L. J.; Kim, G. H. Cell(MC3T3-E1)-printed poly($\epsilon$-caprolactone)/alginate hybrid scaffolds for tissue regeneration. *Macromol. Rapid Commun.* **2013**, *34*, 142−149.
(30) Kim, M. S.; Kim, G. H. Three-dimensional electrospun polycaprolactone (PCL)/alginate hybrid composite scaffolds. *Carbohydr. Polym.* **2014**, *114*, 213−221.
(31) Labet, M.; Thielemans, W. Synthesis of polycaprolactone: A review. *Chem. Soc. Rev.* **2009**, *38*, 3484−3504.
(32) Ahn, S. H.; Kim, Y. B.; Lee, H. J.; Kim, G. H. A new hybrid scaffold constructed of solid freeform-fabricated PCL struts and collagen struts for bone tissue regeneration: fabrication, mechanical properties, and cellular activity. *J. Mater. Chem.* **2012**, *22*, 15901−15909.
(33) Sobral, J. M.; Caridade, S. G.; Sousa, R. A.; Mano, J. F.; Reis, R. L. Three-dimensional plotted scaffolds with controlled pore size gradients: Effect of scaffold geometry on mechanical performance and cell seeding efficiency. *Acta Biomater.* **2011**, *7*, 1009−1018.
(34) Botchwey, E. A.; Dupree, M. A.; Pollack, S. R.; Levine, E. M.; Laurencin, C. T. Tissue engineered bone: Measurement of nutrient transport in three-dimensional matrices. *J. Biomed. Mater. Res.* **2003**, *67A*, 357−367.
(35) Jeon, H.; Kim, G. H. Effect of the internal microstructure in rapid-prototyped polycaprolactone scaffolds on physical and cellular properties for bone tissue regeneration. *Appl. Phys. A: Mater. Sci. Process.* **2012**, *108*, 901−909.
(36) Yeo, M. G.; Simon, C. G.; Kim, G. H. Effects of offset values of solid freeform fabricated PCL-$\beta$-TCP scaffolds on mechanical properties and cellular activities in bone tissue regeneration. *J. Mater. Chem.* **2012**, *22*, 21636−21646.
(37) Murphy, C. M.; Haugh, M. G.; O'Brien, F. J. The effect of mean pore size on cell attachment, proliferation, and migration in collagen−glycosaminoglycan scaffolds for bone tissue engineering. *Biomaterials* **2010**, *31*, 461−466.
(38) Kasemo, B. Biological surface science. *Surf. Sci.* **2002**, *500*, 656−677.
(39) Lord, M. S.; Foss, M.; Besenbacher, F. Influence of nanoscale surface topography on protein adsorption and cellular response. *Nano Today* **2010**, *5*, 66−78.
(40) Gittens, R. A.; McLachlan, T.; Olivares-Navarrete, R.; Cai, Y.; Berner, S.; Tannenbaum, R.; Schwartz, Z.; Sandhage, K. H.; Boyan, B. D. The effects of combined micron/submicron-scale surface roughness and nanoscale features on cell proliferation and differentiation. *Biomaterials* **2011**, *32*, 3395−3403.
(41) Dalby, M. J.; Gadegaard, N.; Tare, R.; Andar, A.; Riehle, M. O.; Herzyk, P.; Wilkinson, C. D. W.; Oreffo, R. O. C. The control of human mesenchymal cell differentiation using nanoscale symmetry and disorder. *Nat. Mater.* **2007**, *6*, 997−1003.
(42) Miller, D. C.; Haberstroh, K. M.; Webster, T. J. Mechanism(s) of increased vascular cell adhesion on nanostructured poly(lactic-*co*-glycolic acid) films. *J. Biomed. Mater. Res., Part A* **2005**, *73*, 476−484.
(43) Jeon, H. J.; Kim, G. H. Effects of a cell-imprinted poly(dimethylsiloxane) surface on the cellular activities of MG63 osteoblast-like cells: Preparation of a patterned surface, surface characterization, and bone mineralization. *Langmuir* **2012**, *28*, 13423−13430.
(44) Jeon, H. J.; Jin, G.; Kim, G. H. The effect of microsized roughness in nano/microsized hierarchical surfaces replicated from a lotus leaf on the activities of osteoblast-like cells (MG63). *J. Mater. Chem.* **2012**, *22*, 7584−7591.
(45) Kubo, K.; Tsukimura, N.; Iwasa, F.; Ueno, T.; Saruwatari, L.; Aita, H.; Chiou, W. A.; Ogawa, T. Cellular behavior on $TiO_2$ nanonodular structures in a micro-to-nanoscale hierarchy model. *Biomaterials* **2009**, *30*, 5319−5329.
(46) Hatano, K.; Inoue, H.; Kojo, T.; Matusunaga, T.; Tsujisawa, T.; Uchiyama, C.; Uchida, Y. Effect of surface roughness on proliferation and alkaline phosphatase expression of rat calvarial cells cultured on polystyrene. *Bone* **1999**, *25*, 439−445.
(47) Chen, H. L.; Li, L. J.; Lin, T. L. Formation of segregation morphology in crystalline/amorphous polymer blends: Molecular weight effect. *Macromolecules* **1998**, *31*, 2255−2264.
(48) Arinstein, A.; Burman, M.; Gendelman, O.; Zussman, E. Effect of supramolecular structure on polymer nanofibre elasticity. *Nat. Nanotechnol.* **2007**, *2*, 59−62.
(49) Halpin, J. C.; Thomas, R. L. Ribbon reinforcement of composites. *J. Compos. Mater.* **1968**, *2*, 488−497.
(50) Peter, S. J.; Miller, M. J.; Yasco, A. W.; Yaszemski, M. J.; Mikos, A. G. Polymer concepts in tissue engineering. *J. Biomed. Mater. Res.* **1998**, *43*, 422−427.
(51) Ishai, O.; Cohen, L. J. Elastic properties of filled and porous epoxy composites. *Int. J. Mech. Sci.* **1967**, *9*, 539−546.
(52) Li, Z.; Ramay, H. R.; Hauch, K. D.; Xiao, D.; Zhang, M. Chitosan−alginate hybrid scaffolds for bone tissue engineering. *Biomaterials* **2005**, *26*, 3919−3928.
(53) Caterson, E. J.; Nesti, L. J.; Li, W. J.; Danielson, K. G.; Albert, T. J.; Vaccaro, A. R.; Tuan, R. S. Three-dimensional cartilage formation by bone marrow-derived cells seeded in polylactide/alginate amalgam. *J. Biomed. Mater. Res.* **2001**, *57*, 394−403.


DOI: 10.1021/co500033h
*ACS Comb. Sci.* 2015, 17, 87−99